

Lossless Convexification of Nonconvex Control Bound and Pointing Constraints of the Soft Landing Optimal Control Problem

Behçet Açıkmüşe, John M. Carson III, and Lars Blackmore

Abstract—Planetary soft landing is one of the benchmark problems of optimal control theory and is gaining renewed interest due to the increased focus on the exploration of planets in the solar system, such as Mars. The soft landing problem with all relevant constraints can be posed as a finite-horizon optimal control problem with state and control constraints. The real-time generation of fuel-optimal paths to a prescribed location on a planet’s surface is a challenging problem due to the constraints on the fuel, the control inputs, and the states. The main difficulty in solving this constrained problem is the existence of nonconvex constraints on the control input, which are due to a nonzero lower bound on the control input magnitude and a nonconvex constraint on its direction. This paper introduces a convexification of the control constraints that is proven to be lossless; i.e., an optimal solution of the soft landing problem can be obtained via solution of the proposed convex relaxation of the problem. The lossless convexification enables the use of interior point methods of convex optimization to obtain optimal solutions of the original nonconvex optimal control problem.

Index Terms—Convex optimization, convexification, interior point method algorithms, optimal control, planetary soft landing.

I. INTRODUCTION

PLANETARY soft landing is one of the benchmark problems of optimal control theory and is gaining renewed interest due to the increased focus on the exploration of planets in the solar system. The main focus of the missions in the near future is to soft-land precisely at scientifically interesting locations, which is also referred to as precision or pinpoint landing. The soft landing is the final phase of a planetary EDL (entry, descent, and landing), and it is also referred to as the powered descent landing stage. In the powered descent stage, the vehicle is guided as close as possible to a prescribed location on the planet’s surface by using thrusters that provide the control authority. This phase concludes when the vehicle lands with zero velocity relative to the surface, i.e., when it

“soft lands.” The problem of designing the fuel-optimal thrust profile as a function of time, which delivers the vehicle as close as possible to a prescribed target under constraints on the thrust and the state of the landing vehicle, is a finite-horizon optimal control problem, and it is referred to as the “soft landing” problem. In this paper, we present an algorithm, which is referred to as the powered descent guidance algorithm, to compute optimal solutions of the soft landing problem based on a lossless convexification of the problem.

Powered descent guidance algorithms minimize the landing error by simultaneously satisfying the constraints such as the governing physics, thrust bounds, and position and speed constraints. Additionally, the short duration of planetary powered descent requires that the guidance algorithms be executed quickly on board in real time and that they guarantee finding a solution when one exists. However, the soft-landing powered-descent guidance problem is a nonconvex finite-horizon optimal control problem in its original form because of the control constraints. The descent thrusters cannot be throttled off after ignition, so the guidance algorithm must generate valid thrust vectors with a nonzero minimum and maximum on the thrust magnitude. This is a nonconvex constraint on the control input. Further, onboard sensors for terrain-relative navigation generally require specific viewing orientations, which constrain the allowable spacecraft orientations and thus the thrust vector pointing direction, which is an additional source of nonconvexity. The main contribution of this paper is to formulate a convex relaxation of the original optimal control problem and show that an optimal solution of the relaxed problem is also optimal for the original one. We refer to this as a lossless convexification of the original control problem, since no part of the feasible region is removed and the optimal solutions of the relaxed problem define optimal solutions to the original problem. Note that many nonconvex optimal control problems can be convexified, but guaranteeing that the convexification is lossless is not always possible. More particularly, one can convexify the problem in two obvious ways: 1) restrict the set of feasible solutions to a convex subset of the feasible set and 2) relax the set of feasible solutions to a convex set containing the original set of feasible solutions. The first approach produces a feasible solution of the original problem with an upper bound on the actual optimal cost, and the second approach generates a lower bound on the optimal cost but, in general, does not necessarily provide a feasible solution of the original problem. Hence the first approach has

Manuscript received January 16, 2012; accepted December 19, 2012. Manuscript received in final form December 27, 2012. Date of publication February 1, 2013; date of current version October 15, 2013. Recommended by Associate Editor N. Hovakimyan.

B. Açıkmüşe is with the Department Aerospace Engineering and Engineering Mechanics, The University of Texas, Austin, TX 78712 USA (e-mail: behcet@austin.utexas.edu).

J. M. Carson is with the Jet Propulsion Laboratory, California Institute of Technology, Pasadena, CA 91109 USA (e-mail: jmcarson@jpl.nasa.gov).

L. Blackmore is with SpaceX Company, Hawthorne, CA 90250 USA (e-mail: lars.blackmore@spacex.com).

Color versions of one or more of the figures in this paper are available online at <http://ieeexplore.ieee.org>.

Digital Object Identifier 10.1109/TCST.2012.2237346

a loss in the optimal cost achievable and the second approach has a loss since it does not necessarily provide a feasible solution. Our convexification follows the second approach, but we guarantee a feasible and, hence, optimal solution of the original problem. Therefore, our convexification of control constraints is lossless. Another source of nonconvexity is having time-varying mass in the dynamics, which is resolved via a change of variables as in [1].

A number of prior works have proposed solutions to variants of the powered descent guidance problem, including [1]–[8], and [9]. In [3], a 1-D version of the soft landing problem is solved analytically in a closed form. However, this solution cannot be extended to the 3-D problem with state or control constraints. One existing solution method is our convex optimization approach [1], [2], which poses the problem of minimum-fuel powered descent guidance as a second-order cone program (SOCP). This optimization problem can be solved in polynomial time using existing interior point method (IPM) algorithms that have a deterministic stopping criterion given a prescribed level of accuracy. That is, the global optimum can be computed to any given accuracy with an *a priori* known upper bound, i.e., a polynomial function of the problem size, on the number of iterations required for convergence. In addition, IPM algorithms of SOCPs are guaranteed to find a feasible solution if one exists [10]–[13]. This is in contrast with other approaches that either compute a closed-form solution by ignoring the constraints of the problem [5], [14], propose solving a nonlinear optimization on board [6], [7], or solve a related problem that does not minimize fuel use [8]. The closed-form solution approaches result in solutions that do not obey the constraints inherent in the problem, such as no subsurface flight constraints. This means that constraints must be checked explicitly after a solution is generated, and any solution that violates the constraints is rejected. In practice, this reduces the size of the region from which return to the target is possible by a factor of five or more [15], and the proposed method is numerically robust as also observed independently [16]. Nonlinear optimization approaches, on the other hand, cannot provide *a priori* guarantees on how many iterations will be required to find a feasible trajectory, and are not guaranteed to find the global optimum, which limits their onboard applicability. For a comparison of the convex optimization approach to alternative approaches, see [9] and [15].

In this paper, we unify the convex optimization approaches of [1], [2], [17] and extend them to handle thrust pointing constraints. While convexifying the problem with nonconvex thrust pointing constraints, we develop a geometrical insight into the problem that establishes a connection with “normal systems” [18]. A normal linear system is defined in the context of optimal control theory where the system is said to be normal with respect a set of feasible controls if it maximizes the Hamiltonian at a unique point of the set of feasible controls. In the case when the set of feasible controls is convex, a system being normal implies that the Hamiltonian is maximized at an extreme point of the set [18]. Our convexification result has a similar geometric interpretation since it establishes lossless convexification by ensuring that the Hamiltonian is maximized

at the extreme points of a projection of the relaxed set of feasible controls. This set is then shown to be contained in the original nonconvex set of feasible controls, thereby establishing that we can obtain optimal solutions of the original nonconvex problem via solving its convex relaxation.

The theoretical development of lossless convexification for the soft landing problem allows the application of IPMs of convex optimization [10]–[12], [19] that can solve these problems reliably with polynomial-time convergence guarantees. Further, a surge of interest in the area of fast real-time convex optimization [20]–[22] has demonstrated computational speedups of several orders of magnitude for IPMs. The advancements in this area will dramatically enhance the real-time computational efficiency of IPMs, thereby enabling their use for planetary soft landing.

A. Partial List of Notations

\mathbb{R} is the set of real numbers; a condition is said to hold almost everywhere in the interval $[a, b]$, a.e. $[a, b]$ if the set of points in $[a, b]$ where this condition fails to hold is in a set of measure zero; \mathbb{R}^n is the n -dimensional real vector space; $\|v\|$ is the 2-norm of the vector v ; $\mathbf{0}$ is a matrix of zeros; I is the identity matrix; e_i is a column vector with its i th entry 1 and other entries zero; (v_1, v_2, \dots, v_m) represents a vector obtained by augmenting vectors v_1, \dots, v_m such that $(v_1, v_2, \dots, v_m) := [v_1^T \ v_2^T \ \dots \ v_m^T]^T$; ∂S denotes the set of boundary points and $\text{int } S$ denotes the interior of the set S .

II. PLANETARY LANDING WITH THRUST POINTING CONSTRAINTS

The planetary soft landing problem searches for the thrust (control) profile T_c and an accompanying translational state trajectory $(\mathbf{r}, \dot{\mathbf{r}})$ which guide a lander from an initial position \mathbf{r}_0 and velocity $\dot{\mathbf{r}}_0$ to a state of rest at the prescribed target location on the planet while minimizing the fuel consumption. The problem considers planets with a constant rotation rate (angular velocity), a uniform gravity field, and negligible aerodynamic forces during the powered-descent phase of landing. When the target point is unreachable from a given initial state, a precision landing problem (or minimum landing error problem) is considered instead, with the objective to first find the closest reachable surface location to the target and second to obtain the minimum fuel state trajectory to that closest point. We formulate a prioritized optimization approach that handles both problems under a unified framework, which is then referred to as the planetary soft landing problem.

In this problem, there are several state and control constraints. The main state constraints are the glide slope constraint on the position vector and an upper bound constraint on the velocity vector magnitude. The glide slope constraint is described in Fig. 1 and is imposed to ensure that the lander stays at a safe distance from the ground until it reaches its target. The upper bound on velocity is needed to avoid supersonic velocities for planets with atmosphere, where the control thrusters can become unreliable. Both of these constraints are convex and fit well to the convex optimization framework considered in this paper. The control constraints,

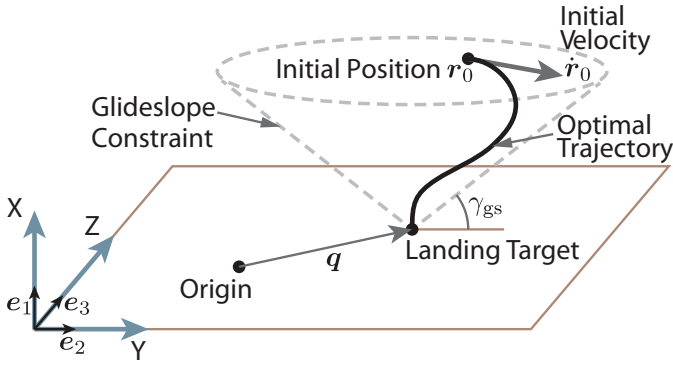


Fig. 1. Glide slope constraint in the minimum landing error powered descent guidance problem. This constraint requires the spacecraft to remain in a cone defined by the minimum slope angle γ . In the minimum landing error case, the apex of the cone coincides with the landed position of the spacecraft, rather than the original target.

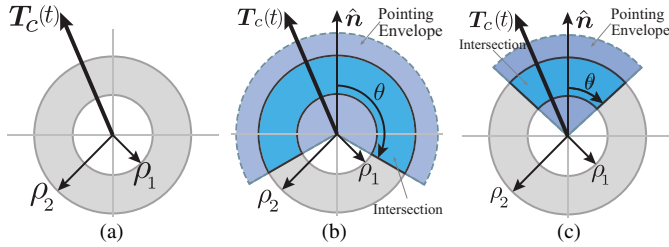


Fig. 2. (a) Planar representation of original thrust bounds, intersection of thrust bounds and thrust pointing limits: (b) $\theta \in (\pi/2, \pi)$ and (c) $\theta \in [0, \pi/2]$.

however, are challenging since they define a nonconvex set of feasible controls. We have three control constraints (see Fig. 2). Given any maneuver time (time of flight) t_f , for all $t \in [0, t_f]$.

- 1) Convex upper bound on thrust, $\|\mathbf{T}_c(t)\| \leq \rho_2$.
- 2) Nonconvex lower bound on thrust, $\|\mathbf{T}_c(t)\| \geq \rho_1 > 0$.
- 3) Thrust pointing constraint $\hat{\mathbf{n}}^T \mathbf{T}_c(t) / \|\mathbf{T}_c(t)\| \geq \cos \theta$ where $\|\hat{\mathbf{n}}\| = 1$ is a direction vector and $0 \leq \theta \leq \pi$ is the maximum allowable angle of deviation from the direction given by $\hat{\mathbf{n}}$, which is convex when $\theta \leq \pi/2$ and nonconvex when $\theta > \pi/2$.

Onboard sensors for terrain-relative navigation generally require specific viewing orientations, which imposes a constraint on the vehicle orientation (attitude). Since we model the vehicle as a point mass with a thrust vector, the required control force is applied by pointing the thrust vector along the desired force direction. In this framework, we can impose constraints on the vehicle orientation by simply restricting the directions that the thrust vector can point to. This also avoids incorporating the attitude dynamics of the vehicle into the problem formulation, which would otherwise increase the problem complexity significantly. Considering attitude dynamics explicitly and imposing the pointing constraints directly, rather than on the thrust direction, can be a part of future research, which can benefit from the recent convexification results on the constrained attitude control [23].

As mentioned earlier, the lander is modeled as a lumped mass with a thrust vector for control, and its dynamics are

described by

$$\begin{aligned} \dot{\mathbf{x}}(t) &= \mathbf{A}(\boldsymbol{\omega}) \mathbf{x}(t) + \mathbf{B} \left(\mathbf{g} + \frac{\mathbf{T}_c(t)}{m(t)} \right) \\ \dot{m}(t) &= -\alpha \|\mathbf{T}_c(t)\| \end{aligned} \quad (1)$$

where $\mathbf{x}(t) = (\mathbf{r}(t), \dot{\mathbf{r}}(t)) : \mathbb{R}_+ \rightarrow \mathbb{R}^6$, $m(t) : \mathbb{R}_+ \rightarrow \mathbb{R}_+$ is the mass of the lander

$$\begin{aligned} \mathbf{A}(\boldsymbol{\omega}) &= \begin{bmatrix} \mathbf{0} & \mathbf{I} \\ -S(\boldsymbol{\omega})^2 & -2S(\boldsymbol{\omega}) \end{bmatrix} \\ \mathbf{B} &= \begin{bmatrix} \mathbf{0} \\ \mathbf{I} \end{bmatrix} \\ S(\boldsymbol{\omega}) &= \begin{bmatrix} 0 & -\omega_3 & \omega_2 \\ \omega_3 & 0 & -\omega_1 \\ -\omega_2 & \omega_1 & 0 \end{bmatrix} \end{aligned} \quad (2)$$

$\boldsymbol{\omega} = (\omega_1, \omega_2, \omega_3) \in \mathbb{R}^3$ is the vector of planet's constant angular velocity, $\mathbf{g} \in \mathbb{R}^3$ is the constant gravity vector, and $\alpha > 0$ is a constant that describes the fuel consumption (mass depletion) rate. Here, the time derivatives of the vectorial quantities are expressed in a planet surface fixed frame that has the planet's angular rotation rate and we also used the rocket equation which relates the fuel mass consumption rate to the applied thrust vector [24].

We use a lumped mass rigid body model of the landing vehicle, where the translational dynamics are decoupled from rotational (attitude) dynamics. This is a common assumption used in practice mainly because the attitude control authority is typically of far higher bandwidth than that of the translational one. Specifically, any attitude maneuver required to point the thruster in the right direction for translational control can be done very quickly such that the interaction between the attitude and translational control systems are minimal. As a result, this is a reasonable assumption that reduces the problem complexity considerably.

Given the constraints, the dynamics, and a target location on the surface $(0, \mathbf{q})$ where $\mathbf{q} \in \mathbb{R}^2$ denotes the coordinates of the target at zero altitude, the planetary soft landing problem can be formulated as a prioritized optimization problem as follows.

Problem 1 (Nonconvex Minimum Landing Error Problem):

$$\min_{t_f, \mathbf{T}_c} \|\mathbf{E}\mathbf{r}(t_f) - \mathbf{q}\| \quad (3)$$

$$\text{s.t. } \left. \begin{aligned} \dot{\mathbf{x}}(t) &= \mathbf{A}(\boldsymbol{\omega})\mathbf{x}(t) + \mathbf{B} \left(\mathbf{g} + \frac{\mathbf{T}_c(t)}{m} \right) \\ \dot{m}(t) &= -\alpha \|\mathbf{T}_c(t)\| \end{aligned} \right\} \quad \forall t \in [0, t_f] \quad (4)$$

$$\mathbf{x}(t) \in \mathbf{X} \quad \forall t \in [0, t_f] \quad (5)$$

$$0 < \rho_1 \leq \|\mathbf{T}_c(t)\| \leq \rho_2, \quad \hat{\mathbf{n}}^T \mathbf{T}_c(t) \geq \|\mathbf{T}_c(t)\| \cos \theta \quad (6)$$

$$m(0) = m_0, \quad m(t_f) \geq m_0 - m_f > 0 \quad (7)$$

$$\mathbf{r}(0) = \mathbf{r}_0, \quad \dot{\mathbf{r}}(0) = \dot{\mathbf{r}}_0 \quad (8)$$

$$\mathbf{e}_1^T \mathbf{r}(t_f) = 0, \quad \dot{\mathbf{r}}(t_f) = \mathbf{0}. \quad (9)$$

Problem 2 (Nonconvex Minimum Fuel Problem):

$$\max_{t_f, \mathbf{T}_c} m(t_f) - m(0) = \min_{t_f, \mathbf{T}_c(\cdot)} \int_0^{t_f} \alpha \|\mathbf{T}_c(t)\| dt \quad \text{s.t.} \quad (10)$$

dynamics and constraints given by (4)–(9)

$$\|\mathbf{E}\mathbf{r}(t_f) - \mathbf{q}\| \leq \|\mathbf{d}_{\rho_1}^* - \mathbf{q}\|. \quad (11)$$

In Problem 2, $\mathbf{d}_{p1}^* = E\mathbf{r}_{p1}^*(t_f) \in \mathbb{R}^2$ is the final position for the optimal cost obtained by solving Problem 1, i.e., \mathbf{d}_{p1}^* is the closest reachable point on the surface to the target location \mathbf{q} , m_f is the available fuel, m_0 is the initial mass of the lander, and

$$E = \begin{bmatrix} \mathbf{e}_2^T \\ \mathbf{e}_3^T \end{bmatrix} = \begin{bmatrix} 0 & 1 & 0 \\ 0 & 0 & 1 \end{bmatrix}.$$

We use \mathbf{X} to define the set of feasible positions and velocities for the spacecraft, i.e., the glide slope constraint, and the maximum allowable speed constraint given by V_{\max}

$$\mathbf{X} = \left\{ (\mathbf{r}, \dot{\mathbf{r}}) \in \mathbb{R}^6 : \|\dot{\mathbf{r}}\| \leq V_{\max}, \|E(\mathbf{r} - \mathbf{r}(t_f))\| - \mathbf{c}^T(\mathbf{r} - \mathbf{r}(t_f)) \leq 0 \right\} \quad (12)$$

where \mathbf{c} specifies a feasible cone with its vertex at $\mathbf{r}(t_f)$

$$\mathbf{c} \triangleq \frac{\mathbf{e}_1}{\tan \gamma_{\text{gs}}}, \quad \gamma_{\text{gs}} \in (0, \pi/2). \quad (13)$$

Here, γ_{gs} is the minimum glide slope angle, as illustrated in Fig. 1. The glide slope constraint (12) ensures that the trajectory to the target cannot be too shallow or go subsurface. \mathbf{X} is a convex set, and for completeness we give the standard definition of the interior of \mathbf{X}

$$\text{int}\mathbf{X} \triangleq \{ \mathbf{x} \in \mathbf{X} : \exists \varepsilon > 0 \text{ such that } \mathbf{y} \in \mathbf{X} \text{ if } \|\mathbf{x} - \mathbf{y}\| < \varepsilon \}. \quad (14)$$

The boundary of \mathbf{X} is given by $\partial\mathbf{X} \triangleq \{ \mathbf{x} \in \mathbf{X} : \mathbf{x} \notin \text{int}\mathbf{X} \}$. Equation (7) defines the initial mass of the lander and ensures that no more fuel than available is used. Equation (8) defines the initial position and velocity of the lander, while (9) constrains the final altitude and the velocity. The time of flight t_f is an optimization variable and is not fixed *a priori*.

The solution of the soft landing problem is obtained by solving Problems 1 and 2. The motivation for this two-step prioritization approach is quite intuitive. The primary goal of planetary landing problem considered in this paper is to land a vehicle as close to a given target as possible, i.e., to minimize the landing error as in Problem 1. There can be multiple optimal solutions for this problem, hence we have a second step where we find the minimum error solution that consumes the least fuel, as in Problem 2.

Remark 1: In Problem 2, the constraint on the final position is given by inequality (11). This constraint could have also been one of the following choices

$$E\mathbf{r}(t_f) = \mathbf{d}_{p1}^* \quad (15)$$

$$\|E\mathbf{r}(t_f) - \mathbf{q}\| = \|\mathbf{d}_{p1}^* - \mathbf{q}\|. \quad (16)$$

And the third choice is the constraint given by (11), which is a convex relaxation of the second choice by including the end positions strictly inside this circle (see Fig. 3). Clearly, we will never be able to compute a solution that has final position strictly inside the circle with this further relaxation because the radius of this circle is the minimum achievable distance to the target. We have two motivations to use the third option: 1) to get the minimum fuel solution that has a final position as close as possible to the desired target and 2) to have all constraints of Problem 2 convex. To see how we

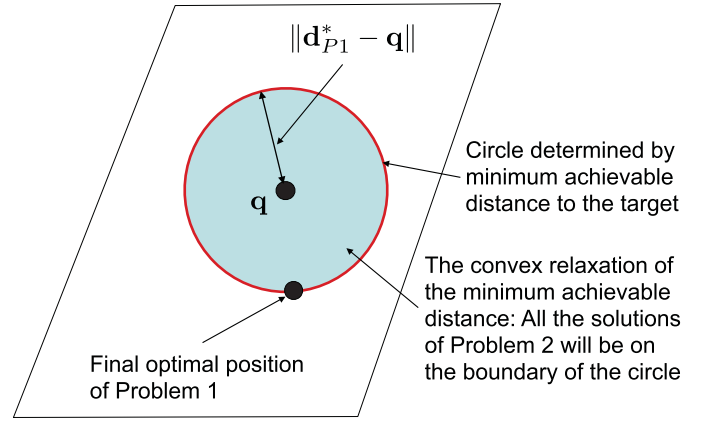


Fig. 3. The convex relaxation of the final position in Problem 2.

achieve both goals, let \mathcal{F}_1 represent all feasible solutions of Problem 2 with (11) replaced by (15); \mathcal{F}_2 is the corresponding set with (11) replaced by (16), and \mathcal{F}_e is the set for Problem 2 as it is. Then it is straightforward to note that $\mathcal{F}_1 \subseteq \mathcal{F}_2 \subseteq \mathcal{F}_e$. Further, we have $\mathcal{F}_2 = \mathcal{F}_e$. This follows from the fact that the inequality (11) does not rule out solutions with end positions on the circle and we cannot get inside the circle. Now, since $\mathcal{F}_1 \subseteq \mathcal{F}_2$, the second option above will produce solutions that use minimal fuel trajectories and end as close as possible to the target. So the best choice is to use the second option. But $\|E\mathbf{r}(t_f) - \mathbf{q}\| = \|\mathbf{d}_{p1}^* - \mathbf{q}\|$ is a nonconvex constraint on the end position. Since $\mathcal{F}_2 = \mathcal{F}_e$, we can simply replace this nonconvex constraint with the convex inequality (11). Consequently, we achieve the two main objectives: 1) to prioritize two costs, the achievable distance and fuel, explicitly, and 2) to convexify both problems so that they can be solved to global optimality in polynomial time via IPM algorithms. Note that we achieve both goals via a systematic prioritization of costs. This kind of prioritization cost in optimization problems is also referred to as lexicographic goal programming [25].

A key challenge in solving Problems 1 and 2 is the lower bound $\rho_1 > 0$ on the thrust magnitude in (6), which means that the set of allowable thrust values is nonconvex (see the first illustration in Fig. 2). Furthermore, when $\rho_1 = 0$, the thrust bound constraint is convex; however, the control constraints can still be nonconvex due to the thrust pointing constraint in (6), which is nonconvex for $\theta > \pi/2$ (see the second and third illustrations in Fig. 2). These nonconvex control constraints prevent the direct use of convex optimization techniques in solving this problem. Additionally, the dynamics for mass consumption $\dot{m}(t)$ in (4) define a nonlinear differential equation, which when discretized leads to nonlinear equality constraints which are also nonconvex.

The key result in [1] includes a relaxation to the nonconvex thrust-bound constraints and an approach to handle the mass consumption dynamics that provided a relaxed version of Problem 2. The optimal solution of this relaxed problem was shown to be also an optimal solution of Problem 2. However, the convexification result of [1] does not hold in the presence of any thrust pointing constraints, including when $\theta \in [0, \pi/2]$. This paper extends the convexification of control

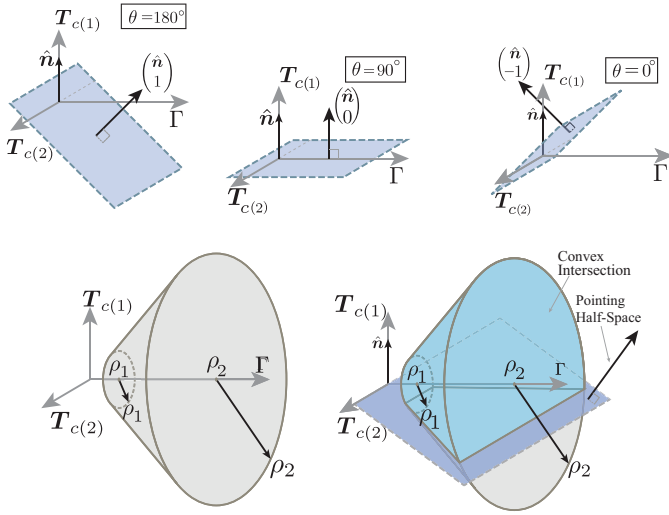


Fig. 4. Relaxed pointing constraint $\mathcal{U}_1 := \{(T_c, \Gamma) : \hat{n}^T T_c \geq \cos \theta \Gamma\}$ is convex, which is illustrated in the first row for a planer case. The set is a half-space in the direction on the normal vector to the planes shown for $\theta = 180^\circ$ (left), $\theta = 90^\circ$ (center), and $\theta = 0^\circ$ (right). Since $\mathcal{U}_2 := \{(T_c, \Gamma) : \|T_c\| \leq \Gamma, \rho_1 \leq \Gamma \leq \rho_2\}$ is also convex, their intersection, $\mathcal{U} = \mathcal{U}_1 \cap \mathcal{U}_2$, defines a convex set of feasible controls for the relaxed problem in $T_c - \Gamma$ space. This is demonstrated in the second row of illustrations for a given θ .

constraints to hold under thrust pointing constraints as well. We also prove that the convexification still holds with the planet's rotation accounted for.

In the relaxed problem, we have the following control constraints:

- 1) convex upper bound on thrust, $\|T_c(t)\| \leq \Gamma(t)$;
- 2) convex thrust pointing constraint $\hat{n}^T T_c(t) \geq \Gamma(t) \cos \theta$;
- 3) convex bounds on the slack variable Γ , $\rho_1 \leq \Gamma(t) \leq \rho_2$.

The relaxed pointing constraint forms a half-space of valid thrust values in $T_c - \Gamma$ space, with pointing in the direction of the outward facing normal to the half space, given by $(\hat{n}, -\cos \theta)$, which comes directly from the relaxed convex pointing-constraint inequality above. The half-space constraint is illustrated for several pointing angles ($\theta = \{180, 90, \text{and } 0^\circ\}$) in Fig. 4, which uses a planar representation of thrust (i.e., 2-D thrust) with a pointing vector \hat{n} along the $T_{c(1)}$ axis. It shows that the relaxed set of constraints is convex.

III. LOSSLESS CONVEXIFICATION

We propose the following relaxed minimum-error and fuel-optimal control problems that are convex relaxations of Problems 1 and 2.

Problem 3 (Convex Relaxed Minimum Landing Error Problem):

$$\min_{t_f, T_c, \Gamma} \|Er(t_f) - q\| \quad \text{subject to (5), (7), (8), (9), and}$$

$$\left. \begin{aligned} \dot{x}(t) &= A(\omega)x(t) + B\left(g + \frac{T_c(t)}{m}\right) \\ \dot{m}(t) &= -\alpha\Gamma(t) \end{aligned} \right\} \quad \forall t \in [0, t_f] \quad (17)$$

$$\|T_c(t)\| \leq \Gamma(t), \quad 0 < \rho_1 \leq \Gamma(t) \leq \rho_2 \quad (18)$$

$$\hat{n}^T T_c(t) \geq \cos \theta \Gamma(t) \quad (19)$$

Problem 4 (Convex Relaxed Minimum Fuel Problem):

$$\min_{t_f, T_c, \Gamma} \int_0^{t_f} \Gamma(t) dt \quad \text{subject to (5), (7), (8), (9), (17), (18),}$$

(19), and

$$\|Er(t_f) - q\| \leq \|d_{p3}^* - q\| \quad (20)$$

where d_{p3}^* is the final optimal position from Problem 3. Note that the nonconvex thrust constraints in (6) for Problems 1 and 2 have been replaced with convex constraints (18) and (19) in Problems 3 and 4. In [1], we showed that constraint relaxation (18) on the thrust bound allows the discrete-time form of Problem 4 to be posed as a convex optimization problem; the same holds true with the addition of the convex thrust-pointing constraint (19). Hence we will not discuss the discretization of this problem in this paper and refer the reader to [1].

Definition 1: \mathcal{F}_e and \mathcal{F}_f denote the sets of feasible solutions of Problems 1 and 2, i.e., $\{t_f, T_c, x, m\} \in \mathcal{F}_e$ if it satisfies all the state (5), control (6), and fuel (7) constraints, dynamics (4), and boundary constraints (8) and (9) of Problem 1, and similarly for \mathcal{F}_f . \mathcal{F}_e^* and \mathcal{F}_f^* are the corresponding set of optimal solutions. \mathcal{F}_{re} and \mathcal{F}_{rf} are the set of feasible solutions $\{t_f, T_c, \Gamma, x, m\}$ for Problems 3 and 4, with \mathcal{F}_{re}^* and \mathcal{F}_{rf}^* the sets of optimal solutions.

Lemma 1: The following hold:

- 1) $\mathcal{F}_f \subseteq \mathcal{F}_e$, $\mathcal{F}_{rf} \subseteq \mathcal{F}_{re}$, $\mathcal{F}_f^* \subseteq \mathcal{F}_e^*$, and $\mathcal{F}_{rf}^* \subseteq \mathcal{F}_{re}^*$;
- 2) if $\{t_f, T_c, \Gamma, x, m\} \in \mathcal{F}_{rf}$ such that $\|T_c(t)\| = \Gamma(t) \quad \forall [0, t_f]$ then $\{t_f, T_c, x, m\} \in \mathcal{F}_f$;
- 3) if $\{t_f^*, T_c^*, \Gamma^*, x^*, m^*\} \in \mathcal{F}_{rf}^*$ such that $\|T_c(t)^*\| = \Gamma^*(t)$ a.e. $[0, t_f^*]$ then $\{t_f^*, T_c^*, x^*, m^*\} \in \mathcal{F}_f^*$.

Proof: The first two relationships in 1) are straightforward to prove. The next two relationships follow from the first two. Consider a subset of \mathcal{F}_{rf} defined as $\bar{\mathcal{F}}_{rf}$ composed of all solutions of \mathcal{F}_{rf} such that $\Gamma(t) = \|T_c(t)\|, \forall t \in [0, t_f]$. Since $\{t_f, T_c, \Gamma, x, m\} \in \bar{\mathcal{F}}_{rf}$, where $\|T_c(t)\| = \Gamma(t)$, satisfies all the dynamics and constraints of Problem 2, $\{t_f, T_c, x, m\} \in \mathcal{F}_f$. This proves 2). Consequently, since the cost functions are identical for Problem 4 with $\|T_c\| = \Gamma$ and Problem 2, the last statement of the theorem follows. ■

To make use of Lemma 1, we need to compute an optimal solution of Problem 4 and check whether $\Gamma(t) = \|T_c(t)\| \forall t \in [0, t_f^*]$ or not. But we do not know ahead of time, before numerically computing the solution, whether this condition will be satisfied or not. The following theorem establishes that this condition will indeed be satisfied in general, with the caveat that the problem may be required to be modified slightly with the introduction of ϵ and $\hat{\omega}$. It also provides a generalization of the earlier results in [1] and [2] to handle thrust pointing constraints as well as nonzero lower bound on the thrust magnitude. Hence it establishes a lossless convexification of the control constraints in the minimum-fuel soft landing problem, Problem 2, and hence Problem 1.

Theorem 1: Consider Problem 4 with ω replaced by $\hat{\omega}$, which is defined as follows:

$$\text{where } \hat{\omega} := \begin{cases} \omega & \text{if } S(\omega)\hat{n} \neq 0, N^T S(\omega)^2 \hat{n} \neq 0 \\ \omega + \epsilon \hat{n}^\perp & \text{if } S(\omega)\hat{n} = 0 \\ \omega + \epsilon \hat{n} & \text{if } S(\omega)\hat{n} \neq 0, N^T S(\omega)^2 \hat{n} = 0 \end{cases} \quad (21)$$

where $\hat{\mathbf{n}}^\perp$ is a unit vector such that $\hat{\mathbf{n}}^T \hat{\mathbf{n}}^\perp = 0$, $\mathbf{N} \in \mathbb{R}^{3 \times 2}$ has its columns spanning the null space of $\hat{\mathbf{n}}^T$, and $\epsilon > 0$ is a (arbitrarily small) real number. Let $\{t_f^*, \mathbf{T}_c^*, \Gamma^*, \mathbf{x}^*, m^*\} \in \mathcal{F}_{rf}^*$ such that the corresponding state trajectory $\mathbf{x}^*(t) \in \text{int}\mathbf{X} \forall t \in [0, t_f^*]$. Then $\{t_f^*, \mathbf{T}_c^*, \mathbf{x}^*, m^*\} \in \mathcal{F}_f^*$ with $\hat{\omega}$.

Proof: This proof uses Lemmas 2 and 3, which are given in the Appendix.

Let $\tilde{\mathbf{q}} := E\mathbf{r}^*(t_f^*)$. Then we can also consider $\{t_f^*, \mathbf{T}_c^*, \Gamma^*, \mathbf{x}^*, m^*\}$ as an optimal fuel solution of Problem 4, where the constraint $\|E\mathbf{r}(t_f) - \mathbf{q}\| \leq \|d_{p1}^* - \mathbf{q}\|$ is replaced by $E\mathbf{r}(t_f) = \tilde{\mathbf{q}}$. So, without loss of any generality, this version of Problem 4 will be used in this proof.

Since $\mathbf{x}^*(t) \in \text{int}\mathbf{X}$ and $m(t) > m_0 - m_f$ for all $t \in [0, t_f]$, the Maximum Principle of optimal control [see [18, Sec. V.3] or [26, Ch. 1]], there exists a constant $\beta \leq 0$ and absolutely continuous function $\lambda : \mathbb{R}_+ \rightarrow \mathbb{R}^6$ and $\eta : \mathbb{R}_+ \rightarrow \mathbb{R}$, the co-state vectors, such that the following conditions hold.

1) *Co-state conditions:* $\forall t \in [0, t_f^*]$

$$(\beta, \lambda(t), \eta(t)) \neq \mathbf{0} \quad (22)$$

$$\dot{\lambda}(t) = -A(\hat{\omega})^T \lambda(t) \quad (23)$$

$$\dot{\eta}(t) = \frac{\lambda(t)^T B \mathbf{T}_c(t)}{m(t)^2}. \quad (24)$$

2) *Pointwise maximum principle:*

$$H(\phi(t)) = M(\mathbf{x}^*(t), m^*(t), \lambda(t), \eta(t)) \text{ a.e. } t \in [0, t_f^*] \quad (25)$$

where $\phi(t) = (t, \mathbf{x}^*(t), m^*(t), \mathbf{T}_c^*(t), \Gamma^*(t), \lambda(t), \eta(t))$ H is the Hamiltonian defined by

$$H(\phi) := \beta \Gamma + \lambda^T (A(\hat{\omega})\mathbf{x} + B(\mathbf{g} + \mathbf{T}_c/m)) - \alpha \Gamma \eta \quad (26)$$

and, by letting $\mathbf{V} := \{(\mathbf{T}_c, \Gamma) \in \mathbb{R}^4 : \|\mathbf{T}_c\| \leq \Gamma, \rho_1 \leq \Gamma \leq \rho_2, \hat{\mathbf{n}}^T \mathbf{T}_c \geq \Gamma \cos \theta\}$

$$M(\mathbf{x}^*, m^*, \lambda, \eta) = \max_{(\mathbf{T}_c, \Gamma) \in \mathbf{V}} H(\phi). \quad (27)$$

3) *Transversality conditions:*

$$\eta(t_f^*) = 0 \text{ and } H(\phi(t_f^*)) = 0. \quad (28)$$

The necessary conditions of optimality 1) and 2) directly follow from the statement of the Maximum Principle. But the transversality condition requires further explanation. Transversality condition implies that (see [18, p. 190, Sec. V.3]), for an optimal solution of the relaxed problem, the vector $\boldsymbol{\psi}$, defined by

$$\boldsymbol{\psi} := \left(H(\phi(0)), H(\phi(t_f^*)), -\lambda(0), -\eta(0), \lambda(t_f^*), \eta(t_f^*) \right)$$

must be orthogonal to the manifold defined by the set of feasible initial and final states described by $(0, t_f, \mathbf{x}_0, m_0, (0, \tilde{\mathbf{q}}, \mathbf{0}), m(t_f^*))$, which is given by $\text{span}\{\mathbf{e}_2, \mathbf{e}_{14}\}$. The above follows from the fact that t_f and $m(t_f)$ are the only free variables in the manifold of boundary conditions. This then implies that $\mathbf{e}_2^T \boldsymbol{\psi} = 0$ and $\mathbf{e}_{14}^T \boldsymbol{\psi} = 0$, i.e., $H(\phi(t_f^*)) = 0$ and $\eta(t_f^*) = 0$. Next we show that

$$\mathbf{y}(t) := B^T \lambda(t) \neq \mathbf{0} \text{ a.e. } [0, t_f^*]. \quad (29)$$

This will be done by contradiction. Suppose that the condition (29) does not hold. Since \mathbf{y} is an output of the system given

by (23), $\mathbf{y}(t) = \mathbf{0}, \forall t \in [0, t_f^*]$, or $\mathbf{y}(t) = \mathbf{0}$ occurs at a countable number of points in $[0, t_f^*]$, which follows from the first conclusion of Lemma 2. Suppose $\mathbf{y}(t) = \mathbf{0} \forall t \in [0, t_f^*]$. Note that the pair $[A(\omega), B]$ is controllable, which follows from the fact that $[B \ A(\hat{\omega})B]$ is an invertible matrix. Hence the pair $(B^T, -A(\hat{\omega})^T)$ is observable. Consequently, $\mathbf{y}(t) = \mathbf{0} \forall t \in [0, t_f^*]$ implies that $\lambda(t) = \mathbf{0} \forall t \in [0, t_f^*]$. Hence $\dot{\eta}(t) = 0 \forall t \in [0, t_f^*]$. Since $\eta(t_f^*) = 0$, this then implies that $\eta(t) = 0 \forall t \in [0, t_f^*]$. These imply $H(\phi(t)) = \beta \Gamma(t)$. Since $H(\phi(t_f^*)) = 0$ and $\Gamma(t) \geq \rho_1 > 0$, this suggests that $\beta = 0$. Therefore, $(\beta, \lambda(t), \eta(t)) = \mathbf{0} \forall t \in [0, t_f^*]$, which is a contradiction with necessary Condition 1) above. Consequently, there are countably many number of points in $[0, t_f^*]$ where $\mathbf{y}(t) = \mathbf{0}$. Since a countable set has measure zero, condition (29) holds.

Since any countable set has measure zero, the second conclusion of Lemma 2 implies that

$$\mathbf{y}(t) \neq -\alpha(t) \hat{\mathbf{n}} \text{ a.e. } [0, t_f^*] \text{ for } \alpha(t) > 0. \quad (30)$$

Since condition (29) holds, a.e. $[0, t_f^*]$ such that $\mathbf{y}(t) \neq \mathbf{0}$, and for a given $\Gamma^*(t)$ an optimal control thrust $\mathbf{T}_c^*(t)$ must satisfy

$$\mathbf{T}_c^*(t) = \operatorname{argmax}_{(\mathbf{T}_c, \Gamma^*(t)) \in \mathbf{V}} \mathbf{y}(t)^T \mathbf{T}_c = \operatorname{argmax}_{\mathbf{T}_c \in \mathbf{U}(\Gamma^*)} \mathbf{y}(t)^T \mathbf{T}_c \quad (31)$$

where $\mathbf{U}(\Gamma) := \{\mathbf{T}_c \in \mathbb{R}^3 : \|\mathbf{T}_c\| \leq \Gamma, \hat{\mathbf{n}}^T \mathbf{T}_c \geq \Gamma \cos \theta\}$. Furthermore, since condition and (30) holds, a.e. $[0, t_f^*]$ such that $\mathbf{y}(t) \neq \mathbf{0}$ and $\mathbf{y}(t) \neq -\alpha(t) \hat{\mathbf{n}}$ for some $\alpha(t) > 0$, the maximizing solution of (31) must be on the boundary point of $\mathbf{U}(\Gamma^*)$ which is also an extremal point of the set $\mathbf{U}(\Gamma^*)$, which follows from Lemma 3. This lemma also implies that all extremal points of the set $\mathbf{U}(\Gamma)$ satisfy $\|\mathbf{T}_c\| = \Gamma$, and hence $\|\mathbf{T}_c^*(t)\| = \Gamma^*(t)$

$$\|\mathbf{T}_c^*(t)\| = \Gamma^*(t) \text{ a.e. } [0, t_f^*] \quad (32)$$

which implies that an optimal solution of the relaxed problem (4) satisfies

$$0 < \rho_1 \leq \|\mathbf{T}_c^*(t)\| \leq \rho_2, \hat{\mathbf{n}}^T \mathbf{T}_c^*(t) \geq \|\mathbf{T}_c^*(t)\| \cos \theta \text{ a.e. } [0, t_f^*].$$

Consequently, $(t_f^*, \mathbf{T}_c^*, \mathbf{x}^*, m^*) \in \mathcal{F}_f$. Since for any $(t_f, \mathbf{T}_c, \mathbf{x}, m) \in \mathcal{F}_f$, $(t_f, \mathbf{T}_c, \|\mathbf{T}_c\|, \mathbf{x}, m) \in \mathcal{F}_{rf}$, an optimal solution of Problem 4 has an optimal cost which is not greater than the optimal cost of Problem 2. This implies that $(t_f^*, \mathbf{T}_c^*, \mathbf{x}^*, m^*) \in \mathcal{F}_f^*$ from Lemma 1. ■

The above theorem states that we can find the optimal solution for Problem 2 by solving its relaxation in Problem 4 for $\hat{\omega}$. Clearly, for $\omega = \hat{\omega}$, we can find the exact optimal solution of the original problem of interest by solving its relaxation. When $\hat{\omega} \neq \omega$, we can find optimal solutions of a problem that can be made arbitrarily close to the problem of interest by simply choosing $\epsilon > 0$ close to zero. Also when $\theta = \pi$, i.e., when there is no pointing constraint, we can use any unit vector for $\hat{\mathbf{n}}$ such that $\omega = \hat{\omega}$. Hence we can find the exact optimal solution of the original problem of interest.

This result has a connection with ‘‘normal systems’’ [18]. A normal linear system is defined in the context of the optimal control theory and a linear system is said to be normal with respect to a set of feasible controls if it maximizes the

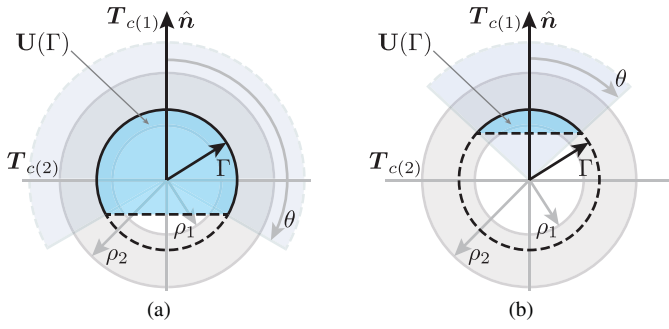


Fig. 5. Planar representation of $\mathbf{U}(\Gamma)$: (a) $\theta \in (\pi/2, \pi)$ and (b) $\theta \in [0, \pi/2]$. Extreme points of $\mathbf{U}(\Gamma)$ satisfy that $\|\mathbf{T}_c\| = \Gamma$, and they are on the solid arc in both figures. The optimal solutions of Problem 4 must be on these extreme points in order to produce feasible, hence optimal, solutions of Problem 2, which is established by Theorem 1.

Hamiltonian at a unique point of the set of feasible controls. In the case when this set is convex, a system being normal implies that the Hamiltonian is maximized at an extreme point of the set of feasible controls (see [18, Coroll. 7.2]). Our convexification result has a similar geometric interpretation since it establishes lossless convexification by ensuring that Hamiltonian is maximized at the extreme points of a projection of the relaxed set of feasible controls. This set is then shown to be contained in the original nonconvex set of feasible controls, thereby establishing that we can obtain optimal solutions for the original nonconvex problem via solving its convex relaxation. The projected set of the relaxed set of controls mentioned above, \mathbf{U} , is given by

$$\mathbf{U}(\Gamma) := \{\mathbf{T}_c \in \mathbb{R}^3 : \|\mathbf{T}_c\| \leq \Gamma, \mathbf{T}_c^T \hat{\mathbf{n}} \geq \cos \theta \Gamma\}.$$

Set \mathbf{U} and its extreme points are shown in Fig. 5 for $\theta \in [0, \pi/2]$ and $\theta \in (\pi/2, \pi)$, and one can observe that its extreme points satisfy $\|\mathbf{T}_c\| = \Gamma$, which results in the convexification of Problem 2 via Problem 4. Indeed, Theorem 1 establishes that any optimal solution of Problem 4 must lie on the extreme points of $\mathbf{U}(\Gamma^*)$, and then the convexification follows from Lemma 1. Note that being in the interior of $\mathbf{U}(\Gamma)$ or on a boundary point that is not an extreme point of $\mathbf{U}(\Gamma)$ can lead to thrust vectors that are not feasible for the original problem, i.e., Problem 2. But, as noted earlier, an extreme point of the set satisfies $\|\mathbf{T}_c\| = \Gamma$ and hence is in the set of feasible controls for Problem 2. Since our result proves that the optimal solution of the relaxed problems occurs at the extreme points, it guarantees that the resulting thrust vectors will always be feasible. Equipped with Lemma 1 and Theorem 1, we propose the following two-step algorithm for the solution of the soft landing problem:

- 1) solve Problem 3 with $\hat{\omega}$ to obtain \mathbf{d}_{P3} ;
- 2) solve Problem 4 with $\hat{\omega}$ and \mathbf{d}_{P3} .

In cases when $\hat{\omega} \neq \omega$, the above algorithm will produce optimal solutions to a problem with dynamics slightly perturbed from the original dynamics. This is necessary for purely theoretical reasons, and we have not yet empirically encountered any case requiring this perturbation of the dynamics.

As mentioned earlier, a more benign source of nonconvexity in the relaxed problems is the existence of $1/m$ term multiplying the thrust vector in the dynamics. This leads to nonlinearity in the dynamics of the system, which then leads to nonconvex equality constraints in the resulting optimization problem. This difficulty will be resolved as described in [1], and is briefly explained in the next subsection.

Both steps above require solutions of the optimal control problems in continuous time. These solutions are obtained by discretizing the problems (with the change of variables given in the next section) to obtain their discrete-time approximations, which are convex parameter optimization problems: more specifically, SOCP problems. SOCPs are solved numerically via IPMs to obtain the solutions of the optimal control problems in both steps. This discretization is explained in [1].

Theorem 1 ensures convexification will hold when the state trajectories are strictly inside the set of feasible states. We observed in our extensive simulations that the result still holds even when the state trajectories intersect with the boundary of the set of feasible states. A proof of this observation is not included here, but will be the topic of a future paper.

It is noteworthy that our convexification result relies on the pair $[A(\hat{\omega}), B]$ being controllable. So, it still applies under system parameter variations as long as this controllability property is preserved. This is clearly not a restrictive condition since it is reasonable to expect that a planetary landing vehicle would be designed to be controllable.

Another important issue is the robustness to uncertainties to unknown parameter variations in the dynamic model or to the disturbance forces. Here we provide a method to compute the optimal state trajectory to be followed and the corresponding optimal controls. Though it is not covered in this paper, one has to consider a feedback control action to handle uncertainties and disturbances. There are several approaches that we can propose to achieve this: 1) to have a tracking feedback controller to follow the optimal state trajectory; 2) to recompute the optimal trajectory and controls as the state knowledge (estimates) are updated during the maneuver; and 3) a combination of tracking feedback and optimal control recomputations. All actions would utilize the current best estimate of the state and would provide the feedback action to minimize the effects of uncertainties and disturbances. The design of a robust feedback action will be another future extension to our current paper.

A natural question is whether the convexification approach here can be extended to other control constraints. Some new results for linear systems are provided in [27], where this convexification procedure is applied to a large class of control constraints. However, there the convexification used the fact that optimal controls are on the boundary points of the relaxed set of controls rather than on the extremal points. With the insight obtained in the current paper on the extremal points of the relaxed set, there can be further generalization to this convexification approach, which can be the subject of future research.

A. Change of Variables

We use the following change of variables on the thrust vector and mass to remove the nonlinearity in the dynamics due to T_c/m : $\sigma \triangleq \frac{\Gamma}{m}$, $\mathbf{u} \triangleq \frac{\mathbf{T}_c}{m}$, $z \triangleq \ln m$.

The mass depletion dynamics can then be rewritten as

$$\dot{z} = \frac{\dot{m}(t)}{m(t)} = -\alpha\sigma(t). \quad (33)$$

The change of variables therefore yields a set of linear equations for the state dynamics. The control constraints, however, are no longer convex. These are now given by

$$\|\mathbf{u}(t)\| \leq \sigma(t) \quad \hat{\mathbf{n}}^T \mathbf{u}(t) \geq \cos\theta \sigma(t) \quad \forall t \in [0, t_f] \quad (34)$$

$$\rho_1 e^{-z(t)} \leq \sigma(t) \leq \rho_2 e^{-z(t)} \quad \forall t \in [0, t_f]. \quad (35)$$

As in [1], we use a second-order cone approximation of the inequalities in (35) that can be readily incorporated into the SOCP solution framework, given by

$$\begin{aligned} \rho_1 e^{-z_0} \left[1 - (z(t) - z_0(t)) + \frac{(z(t) - z_0(t))^2}{2} \right] \\ \leq \sigma(t) \leq \rho_2 e^{-z_0} [1 - (z(t) - z_0(t))] \quad \forall t \in [0, t_f] \end{aligned} \quad (36)$$

where $z_0(t) = \ln(m_0 - \alpha\rho_2 t)$ and m_0 is the initial mass of the spacecraft.

In [1, Lemma 2], it is shown that the approximation of the inequalities in (35) given by (36) always produces a feasible solution of the relaxed problems and is generally very accurate for both parts of the inequality and derives an analytic upper bound on the approximation error. Since this paper's focus is the convexification of the control constraints, we will not go into further details of this approximation and refer the reader to [1] for more details.

IV. NUMERICAL EXAMPLES

This section presents a numerical example to demonstrate the algorithm proposed in the previous section to solve the planetary soft landing problem.

The pointing constraints in the planetary soft landing ensure that the translational maneuver does not require the spacecraft to be oriented outside of a desired pointing cone, which usually results in a reduction in performance. For instance, as the pointing constraints are tightened, the required fuel and flight time generally increase due to the restricted thrust pointing capability. This result will be seen in the following comparison simulations, which make use of an example with the following properties: $m_0 = 2000$ kg, $m_f = 300$ kg, $\rho_1 = 0.2 T_{\max}$, $\rho_2 = 0.8 T_{\max}$, $T_{\max} = 24000$ N, and $\alpha = 5 \times 10^{-4}$ s/m, where T_{\max} is the maximum thrust magnitude. The thrust limits coincide with a minimum and maximum throttle level of 20% and 80%, respectively. A frame of reference, as illustrated in Fig. 1, is used to express the Martian gravity and rotation vector, as well as the spacecraft's initial state conditions at powered-descent ignition. The initial state of the spacecraft for the simulations is given by

$$\mathbf{r}_0 = (2400, 450, -330) \text{ m}, \quad \dot{\mathbf{r}}_0 = (-10, -40, 10) \text{ m/s}$$

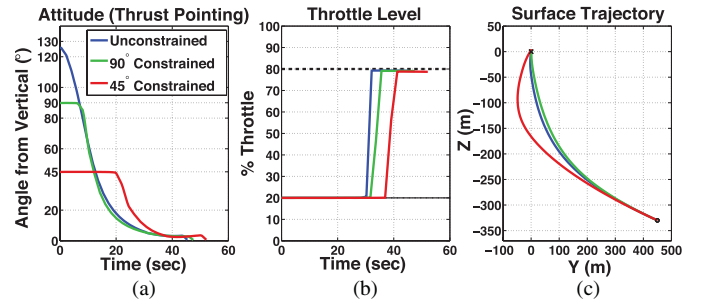


Fig. 6. Simulation results with three different pointing constraints. (a) Unconstrained. (b) $\theta = 90^\circ$. (c) $\theta = 45^\circ$. Thrust pointing and magnitude constraints of Problem 2 are satisfied for the optimal solution of Problem 4, as seen in the first two plots. The last plot is the position trajectory of each solution.

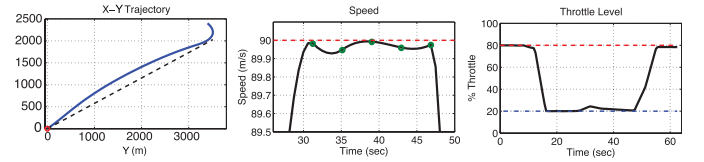


Fig. 7. Example with one contact with the glide slope boundary and two contacts with the speed boundary. The throttle and thrust angle from vertical time profiles (second row) indicate that the thrust vector profile is feasible for Problems 1 and 2, and the convexification still holds, and we obtain an optimal solution to the soft landing problem.

TABLE I
TIGHTENING THRUST POINTING CONSTRAINTS AFFECTING THE FUEL USE AND THE FLIGHT TIME

Attitude	Required Fuel (kg)	Flight Time (s)
Unconstrained	200.1	44.63
90° constraint	201.8	46.96
45° constraint	222.3	57.29

and the target landing site is at $\mathbf{q} = \mathbf{0}$ m, which is the origin of the guidance frame. The Mars gravitational parameters, also expressed in the same coordinate frame are as follows: $\mathbf{g} = (-3.71, 0, 0)$ m/s² and $\boldsymbol{\omega} = (2.53 \times 10^{-5}, 0, 6.62 \times 10^{-5})$ rad/s. Since $S(\boldsymbol{\omega})\hat{\mathbf{n}} \neq \mathbf{0}$ and $\mathbf{N}^T S(\boldsymbol{\omega})^2 \hat{\mathbf{n}} \neq \mathbf{0}$, we have $\hat{\boldsymbol{\omega}} = \boldsymbol{\omega}$. Three simulations were performed for varying pointing-constraint limits: 1) unconstrained; 2) 90° constraint; and 3) 45° constraint. The results of these simulations are overlaid in Fig. 6. As seen in the plot, the pointing angle is relative to local vertical, which aligns the pointing cone $\hat{\mathbf{n}}$ vector along the coordinate frame x -axis. The attitude pointing plot indicates that the solution of the relaxed problem ensures satisfying the prescribed pointing constraints for the original problem. The throttle plot shows that the thrust bounds are satisfied, which indicates that the constraint relaxations in Problem 4 on both thrust magnitude and pointing remain valid for the original problem [Problem 2]. This figure provides some further insight on the tradeoff in performance that occurs as the constraints are tightened. As the pointing limit tightens, the required flight time and fuel increase, as summarized in Table I, which is also visible in the position trajectory. The last plot of Fig. 6 overlays the position trajectories coinciding with the three thrust profiles from the prior figures. The 45° case overshoots the target along the y -axis to satisfy the pointing constraint. Interestingly, the 90° constrained path takes a more direct route.

The next simulation (see Fig. 7) presents a case where the convexification holds with the finite number of contacts with the boundary of \mathbf{X} . In this example, we have the following parameters:

$$\mathbf{r}_0 = (2400, 3400, 0) \text{ m}, \quad \dot{\mathbf{r}}_0 = (-40, 45, 0) \text{ m/s}$$

with a glide slope $\gamma_{\text{gs}} = 30^\circ$ and $\theta = 120^\circ$, with a maximum velocity of 90 m/s.

V. CONCLUSION

This paper presented a lossless convexification of thrust pointing constraints for a benchmark problem in optimal control theory, known as soft landing. This extended and unified our previous work in the area, such that the algorithm could handle upper and lower bounds on thrust, thrust pointing constraints, position and velocity constraints, and planetary rotation. This convexification enables the planetary soft landing problem to be solved optimally by using convex optimization, and is hence amenable to onboard implementation with *a priori* bounds on the computational complexity and realtime execution time.

APPENDIX

Lemma 2: Consider the following linear time invariant system:

$$\begin{aligned} \dot{\boldsymbol{\lambda}}(t) &= -A(\hat{\boldsymbol{\omega}})^T \boldsymbol{\lambda}(t) \\ \mathbf{y}(t) &= B^T \boldsymbol{\lambda}(t) \end{aligned} \quad (37)$$

where $\boldsymbol{\lambda}(t) \in \mathbb{R}^6$ and $\mathbf{y}(t) \in \mathbb{R}^3$, and $A(\hat{\boldsymbol{\omega}})$ and B are given by (2). Then the following conditions hold true; for any finite interval $[0, t_f]$:

- (i) \mathbf{y} is an analytic function, and $\mathbf{y}(t) = \mathbf{0}$ on either $[0, t_f]$ or at countable number of instances;
- (ii) there is a countable number of instances in $[0, t_f]$ such that $\mathbf{y}(t) = \alpha(t)\hat{\mathbf{n}}$ for some $\alpha(t) > 0$.

Proof: $\boldsymbol{\lambda}$, hence \mathbf{y} , are analytic functions of t from [28, Th. 3, p. 213]. Hence $\mathbf{y}(t) = \mathbf{0}, \forall t \in [0, t_f^*]$, or $\mathbf{y}(t) = \mathbf{0}$ occurs at a countable number of points in $[0, t_f^*]$ (Proposition 4.1 on [28, p. 41]). This proves (i).

To prove condition (ii), suppose that there exists an interval $[t_1, t_2] \subseteq [0, t_f^*]$, such that $\mathbf{y}(t) = -\alpha(t)\hat{\mathbf{n}} \forall t \in [t_1, t_2]$, for $\alpha(t) > 0$. Letting $\boldsymbol{\lambda} = (\lambda_1, \lambda_2)$ where $\lambda_{1,2} \in \mathbb{R}^3$, $v_1 := S(\hat{\boldsymbol{\omega}})^T \hat{\mathbf{n}}$ and $v_2 := S(\hat{\boldsymbol{\omega}})^T v_1$, this assumption implies that the following dynamics hold for $t \in [t_1, t_2]$: $\dot{\lambda}_1(t) = -\alpha(t)v_2$ and $\dot{\lambda}_2(t) = -\lambda_1(t) - 2\alpha(t)v_1$.

Due to the construction of $\hat{\boldsymbol{\omega}}$ in Problem 4, we have $v_1 \neq \mathbf{0}$ and $\mathbf{N}^T v_2 \neq \mathbf{0}$. The first inequality is straightforward to show. To see the second one, we need to consider the three cases in (21). First consider the case when $S(\boldsymbol{\omega})\hat{\mathbf{n}} \neq \mathbf{0}$, $\mathbf{N}^T S(\boldsymbol{\omega})^2 \hat{\mathbf{n}} \neq \mathbf{0}$. Then $\boldsymbol{\omega} = \hat{\boldsymbol{\omega}}$ and $\mathbf{N}^T v_2 = \mathbf{N}^T S(\boldsymbol{\omega})^2 \hat{\mathbf{n}} \neq \mathbf{0}$. Second, consider the case when $S(\boldsymbol{\omega})\hat{\mathbf{n}} = \mathbf{0}$, that is, $\boldsymbol{\omega} = a\hat{\mathbf{n}}$ for some $a \in \mathbb{R}$. Then $\hat{\boldsymbol{\omega}} = a\hat{\mathbf{n}} + \epsilon\hat{\mathbf{n}}^\perp$. Then $v_2 = S(\hat{\boldsymbol{\omega}})^T \hat{\mathbf{n}} = S(\hat{\boldsymbol{\omega}})^2 \hat{\mathbf{n}} = \epsilon S(a\hat{\mathbf{n}} + \epsilon\hat{\mathbf{n}}^\perp)S(\hat{\mathbf{n}}^\perp)\hat{\mathbf{n}}$. Since $S(\hat{\mathbf{n}}^\perp)\hat{\mathbf{n}}$ is orthogonal to both $a\hat{\mathbf{n}}$ and $\epsilon\hat{\mathbf{n}}^\perp$, it is orthogonal to their sum, which is nonzero, and hence $v_2 \neq \mathbf{0}$ and it is in the null space of $\hat{\mathbf{n}}^T$. Consequently $\mathbf{N}^T S(\hat{\boldsymbol{\omega}})^T \hat{\mathbf{n}} \neq \mathbf{0}$. Finally, consider the case when $S(\boldsymbol{\omega})\hat{\mathbf{n}} \neq \mathbf{0}$ but $\mathbf{N}^T S(\boldsymbol{\omega})^2 \hat{\mathbf{n}} = \mathbf{0}$. Then we have $S(\hat{\boldsymbol{\omega}})^2 \hat{\mathbf{n}} = S(\boldsymbol{\omega})^2 \hat{\mathbf{n}} +$

$\epsilon S(\hat{\mathbf{n}})S(\boldsymbol{\omega})\hat{\mathbf{n}}$. This has a nonzero component in the nullspace of $\hat{\mathbf{n}}^T$, because $\epsilon S(\hat{\mathbf{n}})S(\boldsymbol{\omega})\hat{\mathbf{n}}$ is nonzero and in the nullspace of $\hat{\mathbf{n}}^T$, and $S(\hat{\boldsymbol{\omega}})^2 \hat{\mathbf{n}}$ is perpendicular to the nullspace of $\hat{\mathbf{n}}^T$. Consequently, we have $\mathbf{N}^T v_2 \neq \mathbf{0}$. Now note that $v_1^T \hat{\mathbf{n}} = 0$. Let v_3 be a nonzero vector such that $v_3^T \hat{\mathbf{n}} = v_3^T v_1 = 0$. Hence v_1 and v_3 span the nullspace of $\hat{\mathbf{n}}$. This implies that we can write $v_2 = c_1 \hat{\mathbf{n}} + c_2 v_3 + c_3 v_1$ for some scalars c_1 through c_3 . Since $v_2^T v_1 = 0$ and $\mathbf{N}^T v_2 \neq \mathbf{0}$ we know that $c_3 = 0$ and $c_2 \neq 0$.

Observe that

$$\dot{\lambda}_2(t) = \lambda_1(t_1) - \int_{t_1}^t \alpha(s)ds v_2 - 2\alpha(t)v_1$$

which implies that

$$\dot{\lambda}_2(t) = \lambda_1(t_1) + g_1(t)\hat{\mathbf{n}} + g_2(t)v_3 - 2\alpha(t)v_1$$

where $g_1(t) = c_1 \int_{t_1}^t \alpha(s)ds$ and where $g_2(t) = c_2 \int_{t_1}^t \alpha(s)ds \neq 0$ for $t \in (t_1, t_2)$. Since v_1, v_3 , and $\hat{\mathbf{n}}$ form an orthogonal set of nonzero vectors, if α is a nonconstant function of time then $\mathbf{N}^T \dot{\lambda}_2(t) \neq 0$ a.e. $[t_1, t_2]$. If α is constant, then g_2 is a nonconstant, linear function of time (since $c_2 \neq 0$), and hence $\mathbf{N}^T \dot{\lambda}_2(t) \neq 0$ a.e. $[t_1, t_2]$. Consequently, $\mathbf{N}^T \dot{\lambda}_2(t) \neq 0$ a.e. $[t_1, t_2]$, which implies that there exists an open finite interval in $[t_1, t_2]$ such that λ_2 will leave the subspace defined by $\hat{\mathbf{n}}$, which is a contradiction caused by assuming that $\lambda_2(t) = -\alpha(t)\hat{\mathbf{n}}$ in $[t_1, t_2]$. Therefore there exists no finite interval where $\mathbf{y}(t) = \lambda_2(t) = -\alpha(t)\hat{\mathbf{n}}$, that is, $\kappa(t) := \mathbf{N}^T \dot{\lambda}_2(t) = \mathbf{0}$. Since κ is analytic function of time (due to $\boldsymbol{\lambda}$ being analytic function of time), either it has a countable number of zeros or there exists time intervals on which it is zero [28]. Since we proved that the latter is not possible, then it must have a countable number of zeros. This concludes the proof. ■

The following lemma is instrumental in the use of Pontryagin's Maximum Principle to show that the optimal control occur at extreme points of a convex feasible set of controls.

Lemma 3: An optimal solution of the following optimization problem is also an extreme point of the feasible set of solutions $\mathbf{U}(\Gamma)$: $\max_{\mathbf{T}_c} \mathbf{y}^T \mathbf{T}_c$ subject to $\mathbf{T}_c \in \mathbf{U}(\Gamma)$ where $\mathbf{U}(\Gamma) := \{\mathbf{T}_c : \|\mathbf{T}_c\| \leq \Gamma, \hat{\mathbf{n}}^T \mathbf{T}_c \geq \cos\theta\Gamma\}$, and $\mathbf{y} \neq \mathbf{0}$ and $\mathbf{y} \neq -a\hat{\mathbf{n}}$ for any $a > 0$. Consequently an optimal solution \mathbf{T}_c^* satisfies that $\|\mathbf{T}_c^*\| = \Gamma$.

Proof: Since the cost function of the optimization problem is linear, hence convex, the maximization problem leads to an optimal solution on the boundary of \mathbf{U} , i.e., on $\partial\mathbf{U}$ [29]. $\partial\mathbf{U}$ has a portion of the sphere with radius Γ and a portion of a hyperplane with unit normal $\hat{\mathbf{n}}$. All extremal points of the boundary are on the sphere: if any point of the boundary is not on the sphere then it is on the hyperplane, on a line segment between two other points of the boundary. This implies that an extremal point of \mathbf{U} satisfies that $\|\mathbf{T}_c\| = \Gamma$.

Note that $\mathbf{y} = c_1 \hat{\mathbf{n}} + c_2 \hat{\mathbf{n}}^\perp$ for some $c_2 \neq 0$ and unit vector $\hat{\mathbf{n}}^\perp$ that is orthogonal to $\hat{\mathbf{n}}$. This implies that $\mathbf{T}_c^* = a_1 \hat{\mathbf{n}} + a_2 \hat{\mathbf{n}}^\perp$ where $a_2 \neq 0$ and $a_1^2 + a_2^2 \leq \Gamma^2$. Suppose that $\hat{\mathbf{n}}^T \mathbf{T}_c^* = \cos\theta\Gamma$, which implies that $a_1 = \cos\theta\Gamma$. Since $\mathbf{y}^T \mathbf{T}_c^* = c_1 a_1 + c_2 a_2 = c_1 \cos\theta\Gamma + c_2 a_2$, the cost is the maximum if c_2 and a_2 has the same sign and the $a_1^2 + a_2^2 = \Gamma^2$, that is, $\|\mathbf{T}_c^*\| = \Gamma$. Consequently an optimal solution must be an extreme point of \mathbf{U} . ■

ACKNOWLEDGMENT

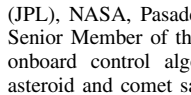
The authors would like to thank M. Ivanov and J. Casoliva of the Jet Propulsion Laboratory for their valuable comments, and S. Boyd, Y. Wang, and J. Mattingley of Stanford University for their insights on convexification and real-time convex optimization. This research was partially performed at the Jet Propulsion Laboratory, California Institute of Technology, under a contract with the National Aeronautics and Space Administration.

REFERENCES

- [1] B. Açıkmeşe and S. R. Ploen, "Convex programming approach to powered descent guidance for mars landing," *Amer. Inst. Astron. Aeron. J. Guid., Control Dyn.*, vol. 30, no. 5, pp. 1353–1366, 2007.
- [2] L. Blackmore, B. Açıkmeşe, and D. P. Scharf, "Minimum landing error powered descent guidance for mars landing using convex optimization," *Amer. Inst. Astron. Aeron. J. Guid., Control Dyn.*, vol. 33, no. 4, pp. 1161–1171, 2010.
- [3] J. S. Meditch, "On the problem of optimal thrust programming for a lunar soft landing," *IEEE Trans. Autom. Control*, vol. 9, no. 4, pp. 477–484, Oct. 1964.
- [4] A. Miele, *The Calculus of Variations in Applied Aerodynamics and Flight Mechanics in Optimization Techniques*, G. Leitmann, Ed. New York: Academic, 1962.
- [5] A. R. Klumpp, "Apollo lunar descent guidance," *Automatica*, vol. 10, no. 2, pp. 133–146, Mar. 1974.
- [6] U. Topcu, J. Casoliva, and K. D. Mease, "Minimum-fuel powered descent for mars pinpoint landing," *J. Spacecraft Rockets*, vol. 44, no. 2, pp. 324–331, 2007.
- [7] R. Sostaric and J. Rea, "Powered descent guidance methods for the moon and mars," in *Proc. AIAA Guid., Navigat., Control Conf.*, Aug. 2005, no. AIAA 2005-6287.
- [8] F. Najson and K. D. Mease, "Computationally inexpensive guidance algorithm for fuel-efficient terminal descent," *J. Guid., Control, Dyn.*, vol. 29, no. 4, pp. 955–964, Jul. 2006.
- [9] B. Steinfieldt, M. Grant, D. Matz, and R. Braun, "Guidance, navigation, and control technology system trades for mars pinpoint landing," in *Proc. AIAA Atmosph. Flight Mech. Conf. Exhibit*, Aug. 2008, no. AIAA 2008-6216.
- [10] S. Boyd and L. Vandenberghe, *Convex Optimal*. Cambridge, U.K.: Cambridge Univ. Press, 2004.
- [11] Y. Nesterov and A. Nemirovsky, *Interior-Point Polynomial Methods in Convex Programming*. Philadelphia, PA: SIAM, 1994.
- [12] J. Peng, C. Roos, and T. Terlaky, *Self-Regularity: A New Paradigm for Primal-Dual Interior-Point Algorithms*. Princeton, NJ: Princeton Univ. Press, 2001.
- [13] J. F. Sturm, "Using sedumi 1.02, a MATLAB toolbox for optimization over symmetric cones," *Optim. Methods Softw.*, vol. 17, no. 6, pp. 1105–1154, 2002.
- [14] C. D'Souza, "An optimal guidance law for planetary landing," in *Proc. AIAA Guid., Navigat. Control Conf.*, 1997, pp. 1376–1381.
- [15] S. Ploen, B. Açıkmeşe, and A. Wolf, "A comparison of powered descent guidance laws for mars pinpoint landing," in *Proc. AIAA/AAS Astrodynamics Special. Conf. Exhibit*, Aug. 2006, no. AIAA 2006-6676.
- [16] B. A. Steinfield, M. J. Grant, D. A. Matz, R. D. Braun, and G. H. Barton, "Guid., navigation and control system performance trades for mars pinpoint landing," *J. Spacecraft Rockets*, vol. 47, no. 1, pp. 188–198, 2010.
- [17] J. M. Carson, B. Açıkmeşe, and L. Blackmore, "Lossless convexification of powered-descent guidance with non-convex thrust bound and pointing constraints," in *Proc. Amer. Control Conf.*, Jun. 2011, pp. 2651–2656.
- [18] L. D. Berkovitz, *Optimal Control Theory*. New York: Springer-Verlag, 1975.
- [19] K. Toh, M. Todd, and R. Tutuncu, "SDPT3—a Matlab software package for semidefinite programming," *Optim. Methods Softw.*, vol. 11, no. 1, pp. 545–581, 1999.
- [20] J. Mattingley and S. Boyd, "Real-time convex optimization in signal processing," *IEEE Signal Process. Mag.*, vol. 27, no. 3, pp. 50–61, May 2010.
- [21] J. Mattingley and S. Boyd, *Automatic Code Generation for Real-Time Convex Optimization. Convex Optimization in Signal Processing and Communications*, Y. Eldar and D. Palomar, Eds. Cambridge, U.K.: Cambridge Univ. Press, 2010.
- [22] Y. Wang and S. Boyd, "Fast model predictive control using online optimization," *IEEE Trans. Control Syst. Technol.*, vol. 18, no. 2, pp. 267–278, Mar. 2010.
- [23] Y. Kim and M. Mesbahi, "Quadratically constrained attitude control via semidefinite programming," *IEEE Trans. Autom. Control*, vol. 49, no. 5, pp. 731–735, May 2004.
- [24] G. P. Sutton and O. Biblarz, *Rocket Propulsion Elements*. New York: Wiley, 2010.
- [25] M. Tamiz, D. Jones, and C. Romero, "Goal programming for decision making: An overview of the current state-of-the-art," *Eur. J. Oper. Res.*, vol. 111, no. 3, pp. 569–581, Dec. 1998.
- [26] L. S. Pontryagin, V. G. Boltyanskii, R. V. Gamkrelidze, and E. F. Mischenko, *The Mathematical Theory of Optimal Processes*. New York: Pergamon, 1964.
- [27] B. Açıkmeşe and L. Blackmore, "Lossless convexification of a class of optimal control problems with non-convex control constraints," *Automatica*, vol. 47, no. 2, pp. 341–347, 2011.
- [28] H. Cartan, *Elementary Theory of Analytic Functions of One or Several Complex Variables*. New York: Dover, 1995.
- [29] L. D. Berkovitz, *Convexity and Optimization in \mathbf{R}^n* . New York: Wiley, 2002.



Behçet Açıkmeşe received the Ph.D. degree in aerospace engineering from Purdue University, West Lafayette, IN, in 2002.



He joined The University of Texas at Austin, Austin, in 2012, where he is currently involved in research on robust and nonlinear control, optimal control, model predictive control, convex optimization, and linear matrix inequalities in guidance, control, and estimation. He was a Visiting Assistant Professor of aerospace engineering with Purdue University. He joined the Jet Propulsion Laboratory (JPL), NASA, Pasadena, CA, in 2003, where he was a Technologist and a Senior Member of the Guidance and Control Analysis Group and developed onboard control algorithms for planetary landing, formation flying, and asteroid and comet sample return.

Dr. Açıkmeşe was a member of the Mars Science Laboratory Controls Team and developed the flight algorithms for the "fly-away" phase of the landing, which were successfully executed during the Mars landing on 5 August 2012.



John M. Carson III received the B.S. degree in aerospace engineering and the M.S. degree in engineering mechanics from the University of Texas at Austin, Austin, in 1997 and 1999, respectively, and the Ph.D. degree in mechanical engineering from the California Institute of Technology, Pasadena, in 2008.

He was with the Lockheed Martin Skunk Works from 1999 to 2000, where he was involved in research on conducting flight and structural dynamics tests and analyses on the Joint Strike Fighter prototype. Since 2001, he has been with the Jet Propulsion Laboratory, NASA, Pasadena, CA, where he is involved on GN&C design, analysis, and hardware development for several missions, including Cassini/Huygens and Mars Exploration Rover, and in research and technology development programs for small-body and planetary landing systems. He currently plays a part in the project management and integration and testing activities with the NASA Autonomous Landing and Hazard Avoidance Technology project that is developing safe precision landing sensors and algorithms for robotic and crewed lander vehicles.



Lars Blackmore received the M.Eng. (Hons.) degree from Cambridge University, Cambridge, U.K., and the Ph.D. degree in aeronautics and astronautics from the Massachusetts Institute of Technology, Cambridge.

He is currently a Senior Guidance, Navigation, and Control Engineer with Space Exploration Technologies (SpaceX), Hawthorne, CA, where he leads the propulsive landing effort, aimed at creating fully reusable spacecraft and he is involved in the development of systems, operations, and algorithms for precision propulsive landing of booster stages and capsules, including the full-scale "Grasshopper" experimental vehicle. He was with the Jet Propulsion Laboratory, NASA, where he was involved in the development of provably optimal algorithms for Mars precision landing, and was a member of the GNC Team for the Soil Moisture Active Passive climate science mission.